Biomaterials 321 (2025) 123332

Contents lists available at ScienceDirect

Biomaterials

journal homepage: www.elsevier.com/locate/biomaterials

Tailoring the therapeutic potential of stem cell spheroid-derived decellularized ECM through post-decellularization BDNF incorporation to enhance brain repair

Ying-Chi Kao [a,1], Pei-Ching Yang [a,1], Yu-Ping Lin [a], Grace H. Chen [a], Shao-Wen Liu [a], Chia-Hsin Ho [a], Shih-Chen Huang [a], Peng-Ying Lee [a], Linyi Chen [b,c], Chieh-Cheng Huang [a,*]

[a] Institute of Biomedical Engineering, National Tsing Hua University, Hsinchu, 30013, Taiwan
[b] Institute of Molecular Medicine, National Tsing Hua University, Hsinchu, 30013, Taiwan
[c] Department of Medical Science, National Tsing Hua University, Hsinchu, 30013, Taiwan

ARTICLE INFO

Keywords:
Cell-derived ECM
Decellularization
Cell spheroid
Traumatic brain injury
Regenerative medicine

ABSTRACT

Decellularized extracellular matrix (dECM) from tissues has significant therapeutic potential but is limited by its rigid molecular composition and reliance on post-decellularization modifications to tailor its functionality. Harsh decellularization processes often result in substantial glycosaminoglycan (GAG) loss, impairing natural growth factor incorporation and necessitating chemical modifications that complicate processing and limit clinical translation. To address these challenges, we developed mesenchymal stem cell (MSC) spheroid-derived three-dimensional (3D) dECM using gentle decellularization techniques. This study demonstrated a crucial advancement—the retention of endogenous GAGs—enabling direct growth factor incorporation without chemical agents. As a proof-of-concept, brain-derived neurotrophic factor (BDNF) was incorporated into the 3D dECM to enhance its therapeutic potential for brain repair. *In vitro*, BDNF-loaded 3D dECM enabled sustained growth factor release, significantly enhancing the proneuritogenic, neuroprotective, and proangiogenic effects. In a mouse model of traumatic brain injury, the implantation of BDNF-loaded 3D dECM significantly enhanced motor function and facilitated brain repair. These findings highlight the adaptability of MSC spheroid-derived 3D dECM for tissue-specific customization through straightforward and translatable growth factor incorporation, demonstrating its potential as a pro-regenerative biomaterial for advancing regenerative medicine applications.

1. Introduction

Traumatic brain injury (TBI) is a globally prevalent neurological disorder and a major public health concern because of its association with profound disabilities and significant socioeconomic burden [1]. Caused by external forces, TBI triggers a cascade of pathological events that lead to post-injury secondary damage, including vascular disruption, excitotoxicity, and neuronal cell death [2]. Clinically, effective strategies to mitigate secondary injury and restore damaged neuronal tissues remain limited because the brain has an inherently low regenerative capacity.

Recently, biomaterial-based therapies have demonstrated promise in reducing secondary cell loss and supporting host neuronal ingrowth, thereby facilitating tissue regeneration [3]. Among these, tissue-derived decellularized extracellular matrix (dECM)—produced by removing cellular and genetic components from native tissues—has demonstrated significant therapeutic potential [4]. By retaining essential ECM components and soluble proteins, tissue-derived dECM mimics native ECM, offering biological cues that enhance brain repair more effectively than that of conventional synthetic biomaterials [5–7].

Despite its promising therapeutic potential, tissue-derived dECM is limited by its xenogeneic origin and fixed molecular composition, which are inherently dictated by the protein and molecular profile of the source tissue before decellularization [8,9]. These inherent limitations restrict the adaptability and customization of tissue-derived dECM, necessitating post-decellularization modifications to optimize bioactivity for therapeutic applications. A common approach is the incorporation of growth factors to enhance the biological functionality of dECM [4]. In

* Corresponding author. Institute of Biomedical Engineering, National Tsing Hua University, Hsinchu, Taiwan.
E-mail address: chiehcheng@mx.nthu.edu.tw (C.-C. Huang).
[1] The first two authors (Y.C. Kao and P.C. Yang) contributed equally to this work.

https://doi.org/10.1016/j.biomaterials.2025.123332
Received 5 January 2025; Received in revised form 6 April 2025; Accepted 7 April 2025
Available online 8 April 2025

native ECM, glycosaminoglycans (GAGs) are crucial for sequestering, protecting, and regulating the release of growth factors that are essential for tissue repair. However, the decellularization process often requires prolonged exposure to harsh detergents, such as sodium dodecyl sulfate (SDS), that can significantly deplete endogenous GAGs and compromise their ability to retain and deliver growth factors effectively [4,10–15]. Therefore, residual GAG levels are often insufficient, necessitating further interventions such as supplementation or covalent modification with exogenous GAGs, like heparin, to restore growth factor binding and release capacities [6,16–26]. For example, brain tissue-derived dECM prepared using a 0.3 % SDS solution over 48 h required heparin modification for the loading and sustained release of nerve growth factors [6]. Although these approaches are effective, they introduce chemical agents, increasing processing complexity and limiting the translational feasibility of tissue-derived dECM-based therapies [15].

To overcome these limitations while leveraging the benefits of tissue-derived dECM, we recently developed an innovative strategy using cell spheroids as the source for dECM production [27]. By assembling human-derived cells into three-dimensional (3D) spheroids followed by gentle decellularization, the resulting cell-derived 3D dECM preserves structural and bioactive properties similar to those of tissue-derived dECM [27,28]. Additionally, this approach offers an allogenic source, eliminating xenogeneic safety concerns and enhancing the translational potential [27,28]. Moreover, the molecular composition of cell-derived 3D dECM can be customized during cell culture, offering greater flexibility for diverse therapeutic applications. When implanted into a mouse TBI model, human mesenchymal stem cell (MSC) spheroid-derived 3D dECM, containing a wealth of MSC secretome, demonstrated significant *in vitro* and *in vivo* pro-regenerative potential by modulating multiple cellular behaviors [28].

Although the MSC secretome retained in 3D dECM supports repair across multiple tissue types, the therapeutic potential of 3D dECM can be further enhanced by incorporating specific growth factors that are naturally present in low amounts. Unlike tissues, cell spheroids, which are only a few hundred micrometers in size, enable efficient decellularization using mild surfactants, such as Triton X-100 (TX-100). This approach enables gentle and rapid decellularization, thereby preserving crucial ECM components and endogenous factors, including significant GAG levels [27], which are essential for growth factor binding and release. Based on this, we hypothesized that MSC spheroid-derived 3D dECM can effectively incorporate growth factors using its endogenous GAG content without requiring chemical modifications.

As a proof-of-concept, this study incorporated brain-derived neurotrophic factor (BDNF)—a neurotrophic factor crucial for nerve repair but limited by its short half-life—into MSC spheroid-derived 3D dECM to enhance its therapeutic efficacy for brain repair. Our *in vitro* results demonstrated that BDNF can be effectively loaded into the 3D dECM and released continuously over two weeks, resulting in significant therapeutic effects, including the suppression of glutamate-induced neuronal cell death, promotion of neurite outgrowth, and stimulation of angiogenesis. In a TBI mouse model, BDNF-loaded 3D dECM-treated animals exhibited significantly enhanced functional outcomes compared with those receiving unmodified 3D dECM. Notably, BDNF loading was achieved without chemical crosslinkers or exogenous agents, highlighting the translational potential of this approach for safe and effective brain repair. Additionally, these findings demonstrate the potential of MSC spheroid-derived 3D dECM as a customizable therapeutic platform for addressing specific repair needs through the targeted delivery of growth factors.

2. Results

2.1. MSC spheroid-derived 3D dECM sequesters BDNF and releases it in a sustained manner

To prepare the 3D dECM, MSCs were assembled into spheroids and subsequently decellularized using a surfactant-based approach with 0.5 % TX-100, as described in our previous studies [27,28]. To demonstrate the advantage of using a mild detergent for cell-derived dECM, a control group was prepared using MSC spheroids decellularized with 0.3 % SDS, a strong detergent commonly used in the preparation of brain tissue-derived dECM [6,29–33]. As illustrated in Fig. 1a, the resulting 3D dECM prepared from both TX-100 and SDS maintained a spherical morphology, with an average diameter of 542.6 ± 41.5 and 529.4 ± 46.7 μm, respectively, closely resembling the diameter of pre-decellularization MSC spheroids (566.1 ± 32.4 μm).

Successful decellularization was confirmed by a marked reduction in the DNA content, with samples prepared using TX-100 or SDS containing 38.8 ± 8.1 ng and 9.2 ± 1.1 ng of DNA per 3D dECM, respectively, compared to 1749.9 ± 393.1 ng per MSC spheroid prior to decellularization (Fig. 1b). These values corresponded to DNA removal efficiencies of 95.9 ± 2.1 % and 99.5 ± 0.2 %, respectively. Hematoxylin and eosin (H&E) staining of cryosectioned samples further confirmed successful decellularization, as no hematoxylin-stained nuclei were observed in either group (Fig. 1c). Both treatments also resulted in a more porous internal architecture, as revealed by H&E staining (Fig. 1c) and scanning electron microscopy (SEM; Fig. 1d). Despite these structural changes, the internal morphology of 3D dECM remained comparable between the TX-100 and SDS groups.

Given our hypothesis that 3D dECM can directly sequester growth factors through its inherent GAGs, similar to native ECM, we initially assessed the retention of the GAG content following decellularization. The Blyscan sulfated GAG assay revealed that each MSC spheroid before decellularization contained 405.1 ± 24.3 pg of GAGs. Following decellularization, GAG content reduced significantly to 187.5 ± 17.1 pg (a 53.7 % reduction) and 65.9 ± 26.5 pg (an 83.7 % reduction) for 3D dECM prepared using TX-100 and SDS, respectively (Fig. 1e). Notably, the use of TX-100 resulted in a 2.9-fold increase in GAG retention compared to that with SDS ($p < 0.005$; Fig. 1e). These findings demonstrated that using a mild detergent (TX-100) in the decellularization procedure for cell spheroid-derived dECM effectively preserves GAGs compared to that using a harsher surfactant (SDS) in tissue-derived dECM preparation, thereby enhancing the capacity of the resulting dECM to sequester and retain growth factors.

Subsequently, we assessed the ability of 3D dECM to load BDNF and compared the BDNF loading capacity of 3D dECM prepared using TX-100 to that prepared using SDS, considering the differences in their GAG content. In this study, the 3D dECM was incubated in phosphate-buffered saline (PBS) containing 100 ng/mL BDNF for 5 h. Following incubation, the BDNF-treated 3D dECM was washed with PBS, lysed, and analyzed using enzyme-linked immunosorbent assay (ELISA) to quantify BDNF levels. Intact MSC spheroids and untreated 3D dECM served as the controls.

As illustrated in Fig. 1f, intact MSC spheroids contained a limited amount of BDNF (3.1 ± 0.2 pg/spheroid), likely produced endogenously during culture. After decellularization, BDNF content reduced significantly to 1.4 ± 0.2 pg (a 55.5 % reduction) and 1.1 ± 0.5 pg (a 63.6 % reduction) for 3D dECM prepared using TX-100 and SDS, respectively (Fig. 1f). This indicated the loss of BDNF and other MSC secretome components during decellularization. Notably, after BDNF treatment, the BDNF content of 3D dECM increased significantly, reaching 830.2 ± 100.3 and 249.3 ± 63.4 pg per 3D dECM prepared using TX-100 and SDS, respectively (Fig. 1f). Importantly, the use of TX-100 resulted in a 3.3-fold increase in BDNF incorporation into the 3D dECM compared to that with SDS ($p < 0.001$; Fig. 1f).

Immunoblot results further confirmed the successful loading of BDNF into the 3D dECM, with BDNF content increasing proportionally to the concentration of the BDNF solution (Fig. 1g). At a BDNF concentration of 100 ng/mL that is commonly used for biomaterial modification in various studies [34–37], the loading efficiency determined using ELISA was 71.2 ± 8.7 % (n = 5 batches). These results confirmed that 3D dECM is an effective platform for loading exogenous growth

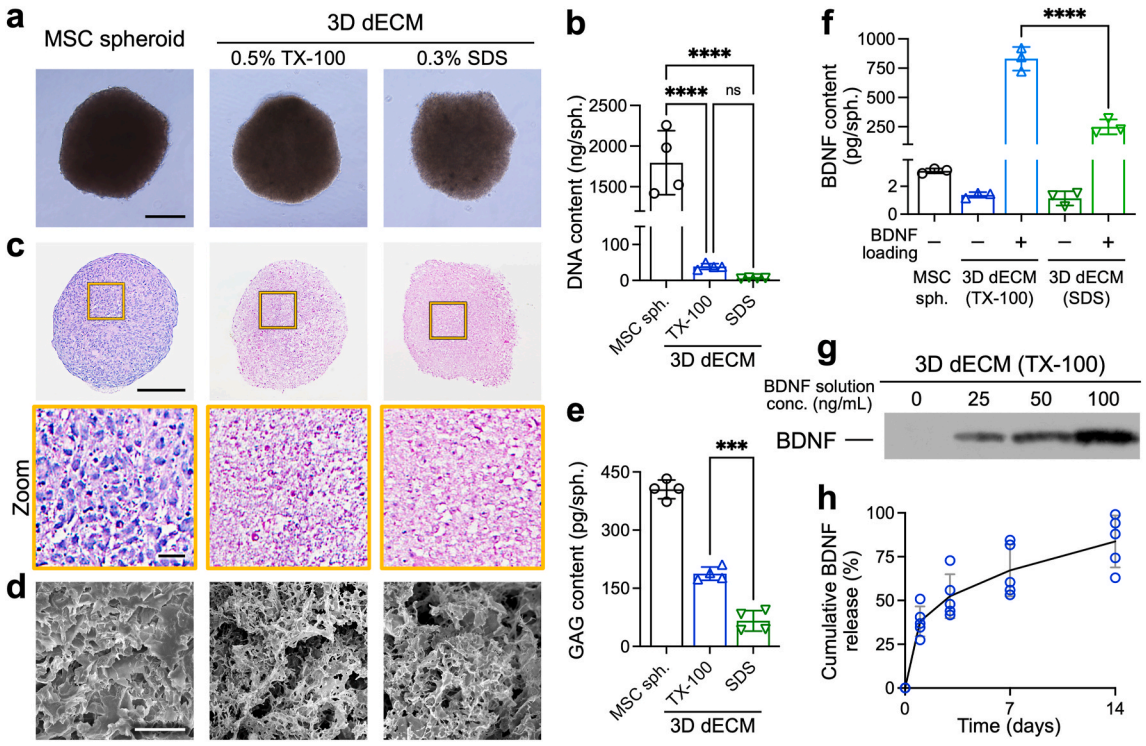

Fig. 1. MSC spheroid-derived 3D dECM retains GAGs and can sequester and release BDNF in a sustained manner. (a) Representative photomicrographs of MSC spheroids and the derived 3D dECM prepared using TX-100 or SDS. Scale bar, 200 μm. (b) DNA content quantified using the PicoGreen assay (n = 4 batches). (c) Representative H&E and (d) SEM images of cryosectioned 3D dECM showing the internal architecture. Scale bar, 200 μm (20 μm for zoomed panel) in (c) and 10 μm in (d). (e) GAG content and (f) BDNF levels in 3D dECM are quantified using the Blyscan GAG assay (n = 4 batches) and ELISA (n = 3 batches), respectively. (g) A representative immunoblot image demonstrating that the level of BDNF incorporation into 3D dECM is proportional to the concentration of BDNF in the loading solution. (h) BDNF-loaded 3D dECM released BDNF in a sustained manner (n = 5 batches). Data are represented as the mean ± standard deviation. Statistical analysis is performed using analysis of variance followed by Tukey's test. ***$p < 0.005$; ****$p < 0.001$; ns, not significant.

factors. Additionally, these findings demonstrated that 3D dECM prepared using a mild detergent (TX-100) has a superior ability to sequester and retain growth factors compared to that prepared using a more aggressive surfactant (SDS) typically used for tissue-derived dECM. Although not the primary objective of the current study, a trend emerged suggesting that larger 3D dECM prepared from MSC spheroids formed using higher cell numbers (Figs. S1a and S1b) may exhibit enhanced BDNF retention (Fig. S1c), likely due to an increased structural volume and GAG content. Further investigation is warranted to clarify this relationship.

Following the confirmation of successful BDNF loading, we assessed its release kinetics by incubating the BDNF-loaded 3D dECM in plain PBS, with periodic collection and analysis of PBS samples using ELISA. As illustrated in the BDNF release profile in Fig. 1h, an initial burst release of BDNF (38.1 ± 8.6 %) was observed on day 1, followed by a gradual release over time. By day 14, approximately 83.7 ± 14.9 % of the loaded BDNF was released, demonstrating the potential of 3D dECM to deliver BDNF in a sustained manner. These findings demonstrated that by leveraging the native potential of ECM, MSC spheroid-derived 3D dECM can effectively load BDNF without additional chemical modification, achieving efficient loading and sustained release, making it a promising carrier system for BDNF delivery in therapeutic applications.

2.2. *BDNF loading enhances the proneuritogenic property of 3D dECM*

After confirming the potential of 3D dECM for BDNF incorporation and delivery, we next investigated whether BDNF loading can further enhance its therapeutic effects. We initially assessed the ability of 3D dECM to support neurite extension, a crucial process for rewiring circuits in injured brain tissues. SH-SY5Y neuroblasts were grown on plates and treated with 3D dECM (with or without BDNF loading), whereas untreated SH-SY5Y cells and those treated with free BDNF served as controls.

Representative fluorescence images detecting class III β-tubulin (Tuj1) (Fig. 2a) and corresponding analyses of average (Fig. 2b) and longest neurite lengths (Fig. 2c) demonstrated that plain 3D dECM-treated neuroblasts exhibited enhanced neurite outgrowth compared to that of untreated controls (78.8 μm *vs.* 59.1 μm for average neurite length, $p < 0.05$; 176.9 μm *vs.* 112.2 μm for longest neurite, $p < 0.01$), likely because of the MSC secretome released from 3D dECM. This effect was further enhanced by BDNF loading, with a 1.5- and 1.8-fold increase in the average ($p < 0.001$) and longest neurite lengths ($p < 0.001$), respectively, highlighting the significant enhancement of the proneuritogenic property of 3D dECM by exogenous BDNF. Additionally, BDNF-loaded 3D dECM demonstrated superior potential in facilitating neurite extension compared to that of treatment with free BDNF, as evidenced by the increased longest neurite length (316.8 μm *vs.* 233.5 μm, $p < 0.001$), likely because of the synergistic effects of exogenously loaded BDNF and endogenously derived MSC secretome.

In addition to acting as a depot for releasing the inherentMSC secretome and loaded BDNF, the 3D dECM, composed entirely of ECM deposited by MSCs, can also function as a scaffold to support tissue regeneration. To evaluate the effect of BDNF loading on scaffold potential, we cultured SH-SY5Y neuroblasts on the surface of 3D dECM, with and without BDNF loading. Fluorescence images of Tuj1 (Fig. 2d) revealed neurite networks on the plain 3D dECM, demonstrating its potential as a scaffold for neuronal cells. In the BDNF-loaded 3D dECM group, more extensive neurite networks developed (Fig. 2d), highlighting the beneficial effects of BDNF loading. These results demonstrated that BDNF loading significantly enhances the proneuritogenic properties of MSC spheroid-derived 3D dECM, providing both physical

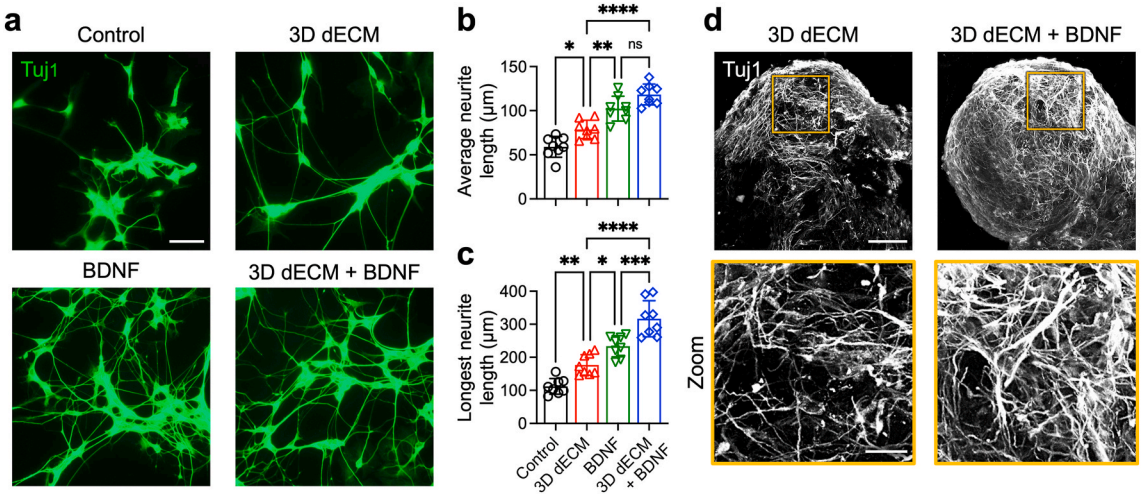

Fig. 2. BDNF loading enhances the proneuritogenic property of 3D dECM. (a) Representative Tuj1 immunofluorescence images illustrating neurite extension from neuroblasts under various treatments, along with (b) average and (c) longest neurite lengths (n = 8). Scale bar, 50 μm. (d) Maximum-intensity projected confocal images demonstrating neurites from SH-SY5Y neuroblasts cultured on 3D dECM with or without BDNF incorporation. Scale bar, 100 μm (30 μm for zoomed panel). Data are represented as the mean ± standard deviation. Statistical analysis is performed using analysis of variance followed by Tukey's test. *$p < 0.05$; **$p < 0.01$; ***$p < 0.005$; ****$p < 0.001$; ns, not significant.

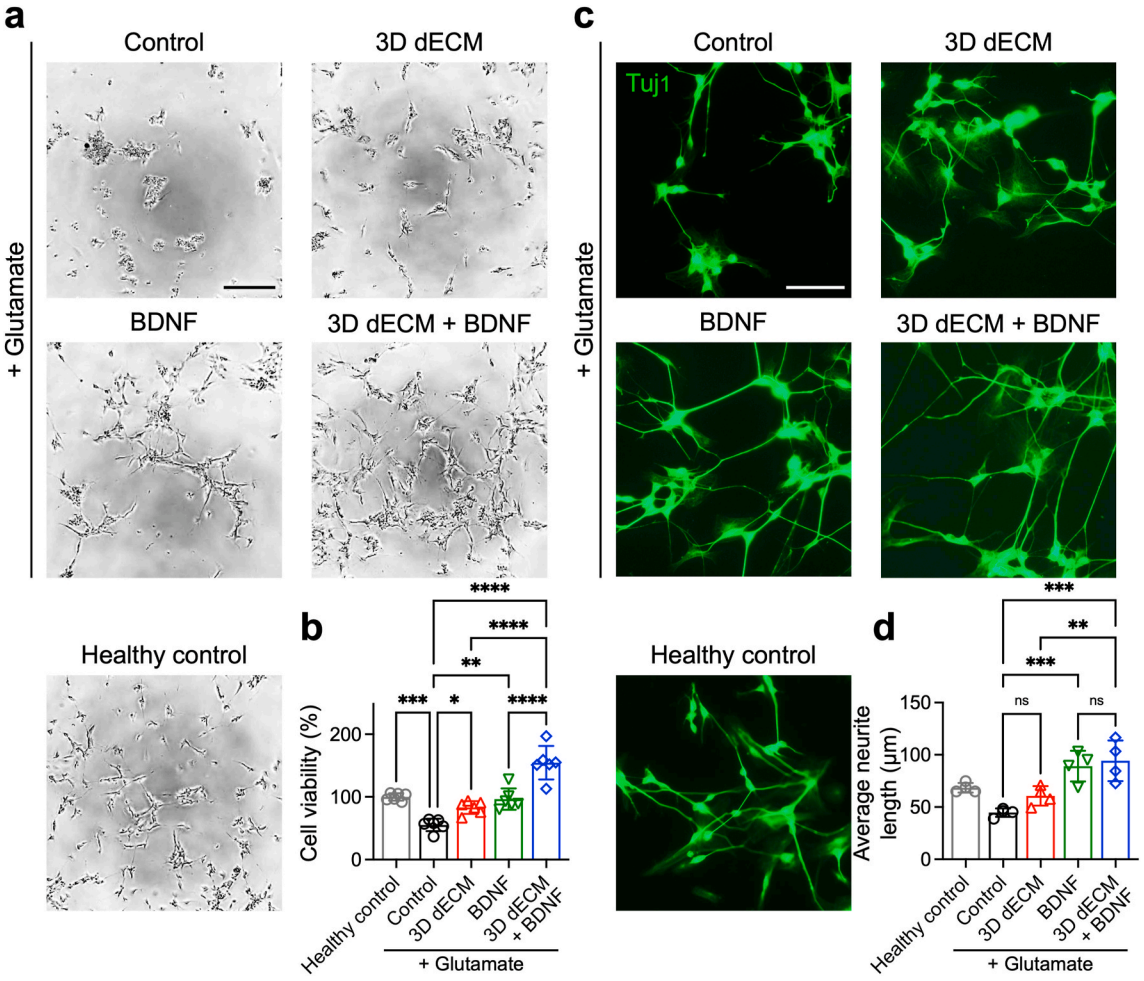

Fig. 3. BDNF loading enhances the neuroprotective potential of 3D dECM. (a) Representative photomicrographs of differentiated neuroblasts cultured in the glutamate-supplemented medium under various treatments, with (b) corresponding cell viability assessed using the CCK-8 assay (n = 6). Scale bar, 200 μm. (c) Representative immunofluorescence images of Tuj1 showing neurite outgrowth from SH-SY5Y neuroblasts cultured in the glutamate-supplemented medium under various treatments, with (d) corresponding measurements of average neurite length (n = 4). Scale bar, 50 μm. Data are presented as the mean ± standard deviation. Statistical analysis is performed using analysis of variance followed by Tukey's test. *$p < 0.05$; **$p < 0.01$; ***$p < 0.005$; ****$p < 0.001$; ns, not significant.

support and biochemical cues to facilitate neurite outgrowth—making it a promising platform for fostering the regeneration of injured brain tissue.

2.3. BDNF loading enhances the neuroprotective and proangiogenic potential of 3D dECM

In addition to supporting neurite outgrowth, an essential role of implant biomaterials at the TBI site is to mitigate secondary cell loss and create a neuroprotective microenvironment to promote subsequent tissue repair. Given the well-documented neuroprotective effects of BDNF, glutamate was used as a model for post-TBI neurotoxicity to determine whether BDNF incorporation augments the ability of 3D dECM to counteract glutamate-induced neuronal damage—a primary contributor to secondary injury following TBI. To this end, SH-SY5Y neuroblasts were treated with glutamate alone or in combination with plain 3D dECM, free BDNF, or BDNF-loaded 3D dECM.

Phase-contrast images (Fig. 3a) and Cell Counting Kit-8 (CCK-8) assay results (Fig. 3b) indicated that glutamate exposure significantly reduced cell density and viability (55.3 % of healthy control; $p < 0.005$). Treatment with plain 3D dECM and free BDNF effectively restored cell viability, with 1.5- and 1.7-fold increases ($p < 0.05$ and $p < 0.01$ *vs.* untreated control, respectively). However, treatment with BDNF-loaded 3D dECM produced a significant effect, achieving a 2.7-fold increase compared to that of the untreated control ($p < 0.001$ *vs.* untreated control, plain 3D dECM, and free BDNF groups).

Additionally, we observed that neurite morphology—which can be compromised by glutamate treatment—was preserved by these treatments (Fig. 3c and d). Specifically, treatment with plain 3D dECM and free BDNF protected neurites, resulting in 1.3- and 1.9-fold increases in average neurite length, respectively. Furthermore, BDNF-loaded 3D dECM achieved a 2.1-fold increase in the average neurite length compared to that of the untreated control ($p < 0.005$; $p < 0.01$ *vs.* plain 3D dECM). These findings demonstrated that BDNF loading significantly enhances the neuroprotective ability of 3D dECM, effectively increasing neuronal cell viability under glutamate-induced stress and preserving neurite integrity.

Although the difference in average neurite length between the free BDNF and BDNF-loaded 3D dECM groups was not statistically significant ($p > 0.05$; Fig. 3d), this is likely attributable to the *in vitro* experimental setup, where free BDNF was directly introduced into the culture medium, ensuring immediate availability and maximal bioactivity in a confined environment. However, in an *in vivo* setting, free BDNF is prone to rapid diffusion and clearance, potentially leading to reduced bioavailability and diminished therapeutic efficacy at the injury site. In contrast, 3D dECM may serve as a localized and sustained delivery platform, leveraging the intrinsic ECM-binding properties to prolong BDNF retention, regulate its release kinetics, and potentially improve therapeutic outcomes.

Because ischemia is another crucial factor in post-TBI brain tissue injury, we assessed the effect of BDNF loading on the proangiogenic potency of the 3D dECM. To evaluate this, human umbilical vein endothelial cells (HUVECs) were cultured on growth factor-reduced Matrigel in serum-containing medium without additional growth factor supplementation for the tube formation assay. After the formation of initial tubular networks, plain 3D dECM, free BDNF, or BDNF-loaded 3D dECM was added to the culture. Phase-contrast images of the tubular structures formed by HUVECs (Fig. 4a) and the corresponding quantitative analysis of the tubular length (Fig. 4b) demonstrated that all groups had similar tubular lengths and morphologies before treatment. Over time, the tubular networks regressed rapidly, which was expected due to the absence of additional growth factor supplementation in the culture medium. However, supplementation with plain 3D dECM and free BDNF effectively mitigated tubular disassembly at both 4 and 24 h ($p < 0.01$ and $p < 0.05$ *vs.* untreated control, respectively)—indicating that both the MSC secretome in 3D dECM and the exogenously loaded BDNF exhibit proangiogenic potential. Notably, BDNF-loaded 3D dECM demonstrated even greater efficacy in maintaining tubular structures ($p < 0.01$ *vs.* plain 3D dECM and free BDNF at 4 h; $p < 0.01$ *vs.* plain 3D dECM and $p < 0.05$ *vs.* free BDNF at 24 h), indicating the superior

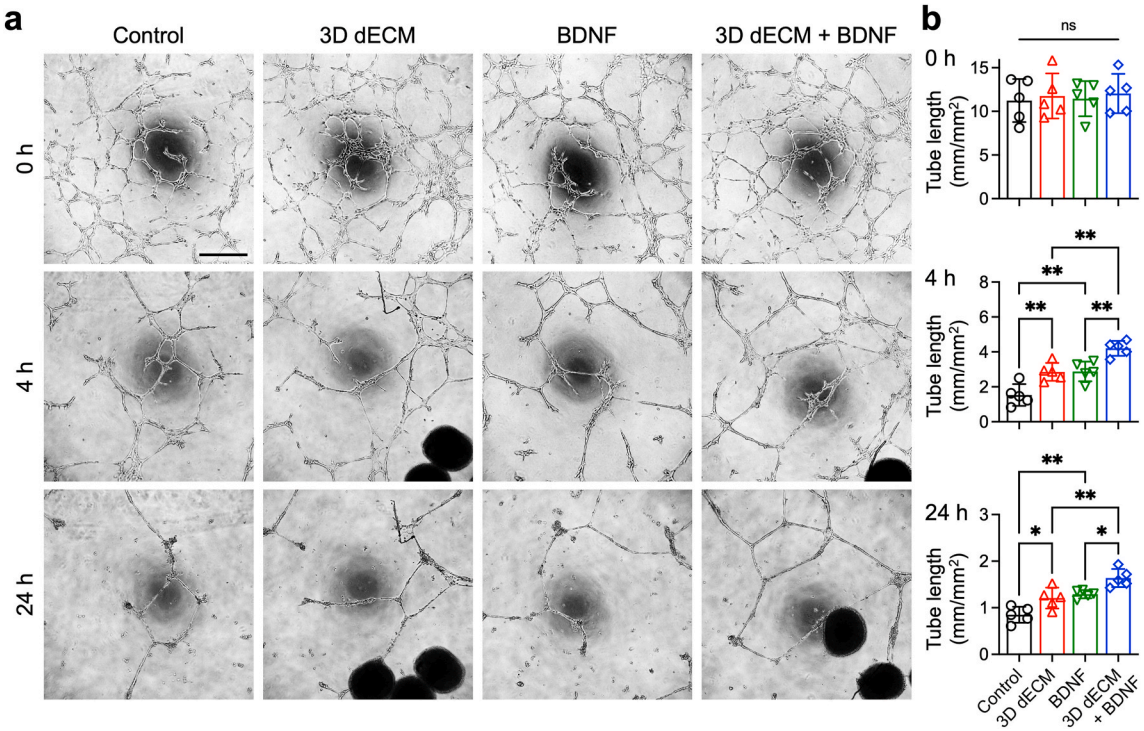

Fig. 4. BDNF loading enhances the proangiogenic potential of 3D dECM. (a) Representative photomicrographs of tubular structures formed on Matrigel by HUVECs under various treatments, with (b) corresponding tube length measurements at different time points (n = 5). Scale bar, 500 μm. Data are presented as the mean ± standard deviation. Statistical analysis is performed using analysis of variance followed by Tukey's test. *$p < 0.05$; **$p < 0.01$; ns, not significant.

potential of BDNF-loaded 3D dECM to facilitate angiogenesis.

Collectively, our *in vitro* findings demonstrated that BDNF loading effectively tailors the therapeutic potential of MSC spheroid-derived 3D dECM by facilitating neurite outgrowth, preventing neuronal cell death, and inducing angiogenesis. These effects highlight its potential as a biomaterial to support brain tissue repair following TBI.

2.4. BDNF loading enhances the efficacy of 3D dECM implantation in mitigating brain injury and improving motor function in TBI mice

After confirming that BDNF loading enhanced the therapeutic effectiveness of 3D dECM *in vitro*, we assessed its potential for brain repair *in vivo* using a mouse TBI model generated through controlled cortical impact (CCI). The BDNF-loaded 3D dECM was implanted on the surface of the cerebral tissue at the site of impact and secured with fibrin gel [28]. Control groups received fibrin gel alone (untreated control), plain 3D dECM (secured with fibrin gel), or fibrin gel containing free BDNF.

Although CCI did not immediately create a significant cavity in the mouse brain, gross examination at 14 days post-injury (dpi) revealed an apparent lesion in the control group, which received fibrin gel as the sole treatment, indicating progressive secondary injury and tissue atrophy post-TBI. Notably, lesion size was markedly smaller in mice receiving plain 3D dECM or BDNF-loaded 3D dECM compared to untreated controls (Fig. 5a). These findings were corroborated by cresyl violet-stained images (Fig. 5b) and the corresponding quantitative analysis of brain lesion volume (Fig. 5c). Although free BDNF treatment did not significantly reduce lesion volume compared to the untreated control (23.3 ± 5.2 % *vs.* 27.1 ± 3.9 %, $p > 0.05$), a significant reduction in lesion volume was observed in mice treated with 3D dECM (19.1 ± 3.6 %, $p < 0.05$) and BDNF-loaded 3D dECM (15.3 ± 3.0 %, $p < 0.01$). However, BDNF loading did not further enhance the ability of 3D dECM to mitigate the progression of post-TBI brain injury and reduce lesion volume compared to that of plain 3D dECM ($p > 0.05$).

In addition to assessing brain lesion volume, we next evaluated the effect of BDNF loading on the therapeutic potential of 3D dECM in

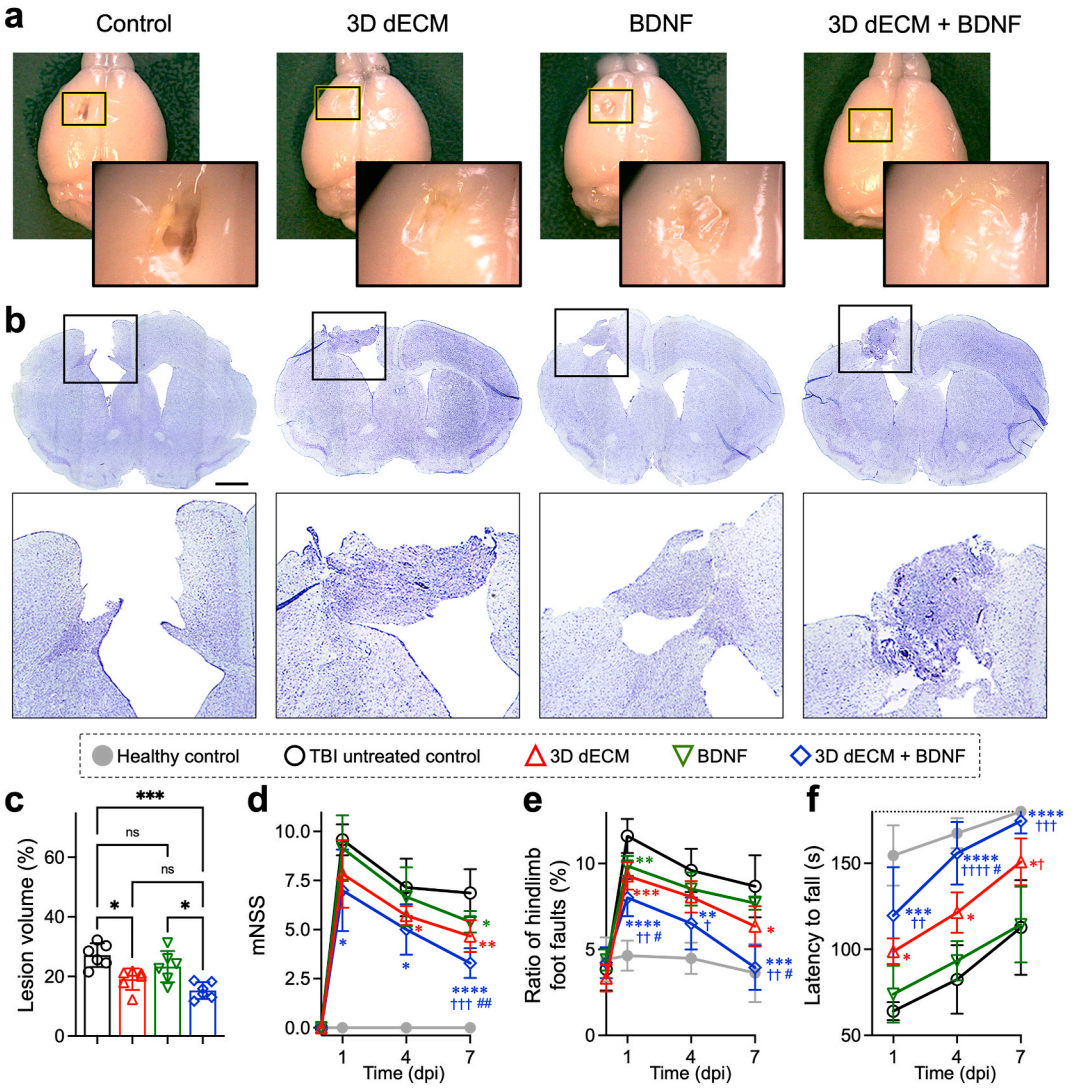

Fig. 5. BDNF loading enhances the therapeutic efficacy of 3D dECM implantation in alleviating brain damage and improving motor function in TBI mice. (a) Representative gross morphology of treated brains and (b) cresyl violet-stained brain sections, with (c) corresponding lesion volume quantification at 14 dpi (n = 6). Scale bars, 1 mm $^{*}p < 0.05$; $^{***}p < 0.005$; ns, not significant. Motor function in the TBI model is assessed using (d) mNSS, (e) hindlimb footfault ratio during grid walking, and (f) duration before falling from a rotating rod (n = 6). $^{*}p < 0.05$, $^{**}p < 0.01$, $^{***}p < 0.005$, $^{****}p < 0.001$ *vs.* TBI untreated control; $^{\dagger}p < 0.05$, $^{\dagger\dagger}p < 0.01$, $^{\dagger\dagger\dagger}p < 0.005$, $^{\dagger\dagger\dagger\dagger}p < 0.001$ *vs.* free BDNF-treated group; $^{\#}p < 0.05$, $^{\#\#}p < 0.01$ *vs.* plain 3D dECM-treated group. Data are presented as the mean ± standard deviation. Statistical analysis is performed using analysis of variance followed by Tukey's test. (For interpretation of the references to color in this figure legend, the reader is referred to the Web version of this article.)

enhancing post-TBI motor function in mice, using the modified neurological severity score (mNSS; Fig. 5d), grid walking (Fig. 5e), and rotarod test (Fig. 5f). After inducing TBI in the sensorimotor cortex, we observed significantly impaired motor function, with higher mNSS scores and increased hindlimb footfaults at 1 dpi. Over time, untreated control animals receiving only fibrin gel showed spontaneous recovery of neurological function across all tasks, potentially because of endogenous reparative mechanisms. Free BDNF treatment provided certain early benefits, notably a reduced footfault ratio at 1 dpi (9.9 ± 0.6 % *vs.* 11.6 ± 1.0 % in untreated control; $p < 0.01$)—but overall resulted in limited enhancement of motor recovery by 7 dpi. This was evidenced by a slight enhancement in mNSS (5.4 ± 0.6 *vs.* 6.9 ± 1.2 in untreated control; $p < 0.05$) and statistically insignificant alterations in both footfault rate during grid walking (6.4 ± 1.2 % *vs.* 8.7 ± 1.8 %; $p > 0.05$) and latency to fall in the rotarod task (114.3 ± 22.0 s *vs.* 112.8 ± 27.5 s; $p > 0.05$).

Implantation of plain 3D dECM significantly improved neurological function across all tasks at 7 dpi (mNSS: 4.7 ± 0.8, footfault rate: 6.3 ± 1.2 %, and latency to fall: 150.9 ± 13.6 s; $p < 0.01$, $p < 0.05$, and $p < 0.05$ *vs.* untreated control, respectively), demonstrating the therapeutic potential of 3D dECM *in vivo*. Notably, BDNF loading further enhanced these improvements in neurological function at 7 dpi (mNSS: 3.3 ± 0.7 and footfault rate: 3.9 ± 1.3 %; $p < 0.01$ and $p < 0.05$ *vs.* plain 3D dECM, respectively), with treated mice remaining on the rotarod for 174.7 ± 7.2 s, approaching the maximum test duration of 180 s. In summary, although MSC spheroid-derived 3D dECM alone provided significant benefits in limiting the spread of post-injury brain damage, BDNF loading significantly enhanced its therapeutic effectiveness in facilitating motor function recovery following TBI.

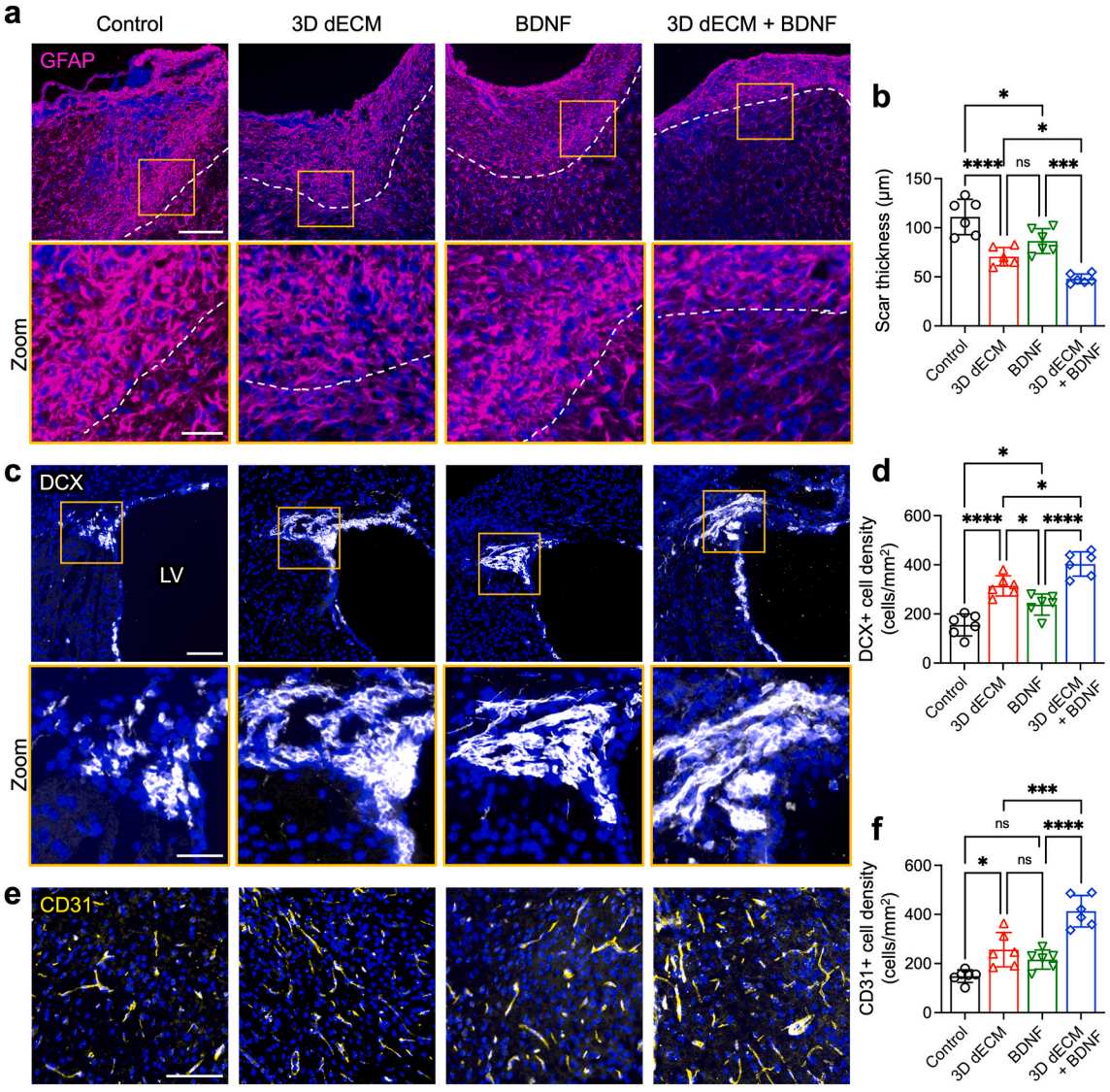

Fig. 6. BDNF loading enhances the ability of 3D dECM implantation to mitigate post-TBI glial scarring, activate neuroblasts, and facilitate angiogenesis in the perilesion area. (a) Representative immunofluorescence images of GFAP staining showing astrocytes, with (b) corresponding quantification of glial scar thickness at 14 dpi (n = 6). Dotted lines indicate the scar tissue borders. Scale bar, 300 μm (40 μm for zoomed panel). (c) Representative immunofluorescence images of DCX staining showing neuroblasts, with (d) corresponding quantification of neuroblast density at 14 dpi (n = 6). LV: lateral ventricle. Scale bar, 100 μm (40 μm for zoomed panel). (e) Representative immunofluorescence images of CD31 staining showing vascular endothelial cells, with (f) corresponding quantification of endothelial cell density at 14 dpi (n = 6). Scale bar, 100 μm. Data are presented as the mean ± standard deviation. Statistical analysis is performed using analysis of variance followed by Tukey's test. *$p < 0.05$; ***$p < 0.005$; ****$p < 0.001$; ns, not significant.

2.5. BDNF loading enhances the ability of 3D dECM implantation to alleviate post-TBI glial scarring, activate neuroblasts, and induce angiogenesis in the peri-lesion area

Following our investigation into the benefits of BDNF loading on 3D dECM in reducing gross brain lesion volume and facilitating motor function recovery, we further explored its effects at the tissue level, focusing on the biological functions commonly associated with BDNF. First, we assessed glial scarring at 14 dpi using fluorescence labeling of glial fibrillary acidic protein (GFAP). As illustrated in the representative fluorescence images (Fig. 6a) and corresponding quantitative analysis of scar thickness (Fig. 6b), free BDNF treatment moderately reduced scar thickness (86.4 ± 12.7 μm *vs.* 111.0 ± 18.1 μm in untreated control; $p < 0.05$). In contrast, 3D dECM implantation significantly reduced glial scarring (70.6 ± 9.2 μm; $p < 0.001$ *vs.* untreated control). Additionally, animals treated with BDNF-loaded 3D dECM exhibited an even greater reduction in glial scar formation (48.2 ± 4.9 μm; $p < 0.001$ *vs.* untreated control; $p < 0.05$ *vs.* plain 3D dECM), indicating a synergistic therapeutic effect between the MSC secretome retained within 3D dECM and the exogenously loaded BDNF.

Beyond alleviating glial scarring, BDNF is known to promote neuroblast activation and migration, processes essential for neural regeneration [38]. To assess this, we performed immunofluorescence staining for doublecortin (DCX) to identify the neuroblasts. Analysis of

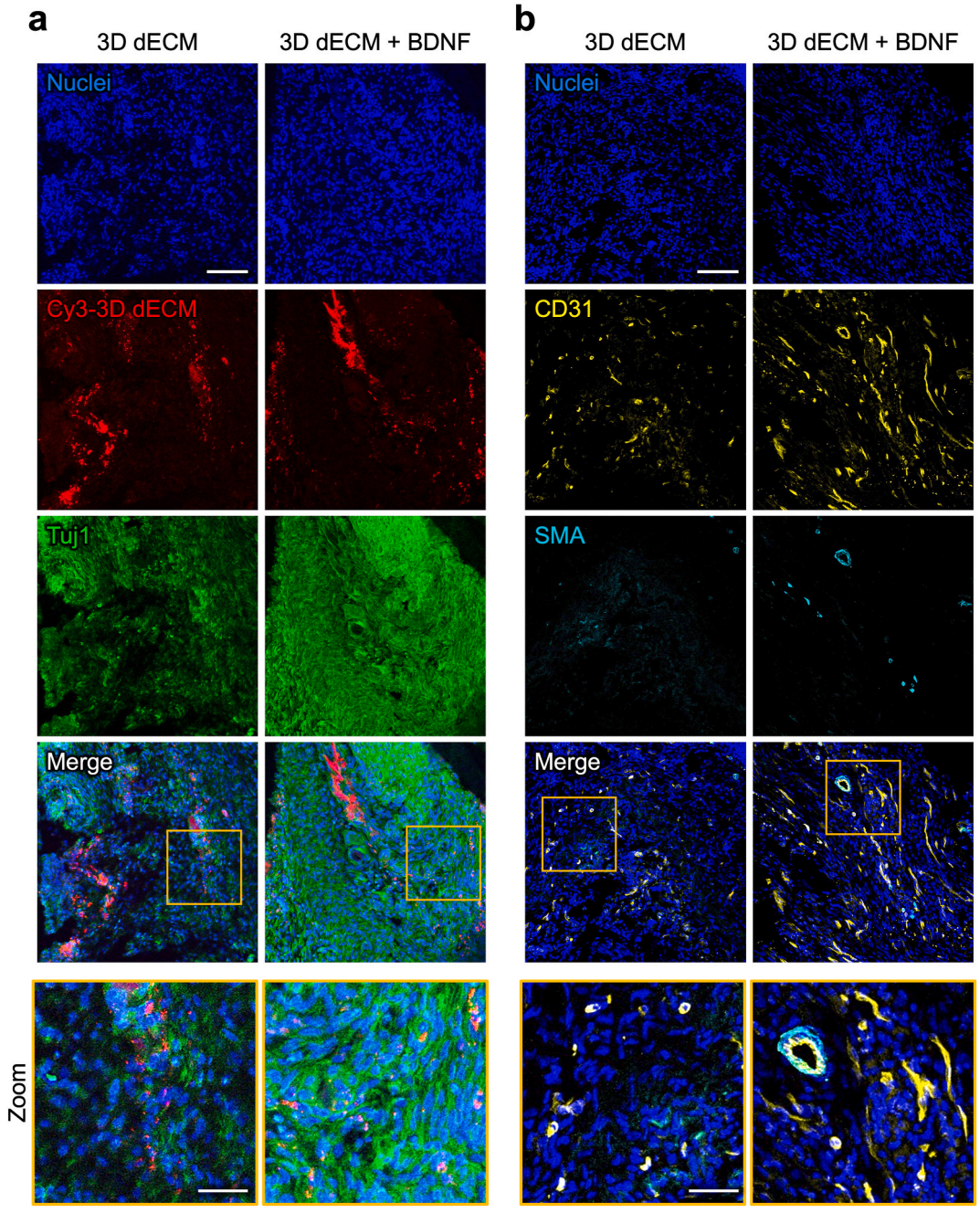

Fig. 7. BDNF loading enhances the ability of 3D dECM to preserve vascularized nerve tissue at the cortical lesion site. (a) Representative fluorescence images showing Cy3-labeled 3D dECM, with or without BDNF incorporation, and Tuj1-positive neuronal cells at 14 dpi. (b) Representative fluorescence images showing CD31-positive vascular endothelial cells and smooth muscle actin (SMA)-positive smooth muscle cells at the implantation site at 14 dpi. Scale bar, 100 μm (40 μm for zoomed panel).

DCX-positive neuroblasts (Fig. 6c) and corresponding quantitative data (Fig. 6d) demonstrated that 3D dECM implantation significantly increased the density of DCX-positive cells in the subventricular zone (SVZ) compared to that of untreated controls (314.2. ± 41.3 cells/mm^2 *vs.* 155.1 ± 44.6 cells/mm^2; $p < 0.001$). Notably, BDNF loading further enhanced this effect, with BDNF-loaded 3D dECM resulting in the highest density of DCX-positive cells (403.3 ± 49.6 cells/mm^2; $p < 0.05$ *vs.* plain 3D dECM). These results highlight the crucial role of BDNF in augmenting the pro-neuroregenerative potential of the 3D dECM.

Another primary mechanism of BDNF-mediated brain repair is its ability to stimulate angiogenesis that enhances local blood perfusion and supports subsequent repair processes. To assess this, we performed immunostaining for CD31 to assess vascularization around the lesion site. The group that received plain 3D dECM demonstrated a marked rise in the density of CD31-positive vascular endothelial cells compared to untreated controls (256.3 ± 69.7 cells/mm^2 *vs.* 148.5 ± 25.6 cells/mm^2 in untreated control; $p < 0.05$; Fig. 6e and f). BDNF loading further enhanced this effect, resulting in a significantly higher density of CD31-positive cells (413.1 ± 63.9 cells/mm^2; $p < 0.005$ *vs.* plain 3D dECM). In summary, these results demonstrated that BDNF loading significantly enhances the therapeutic ability of 3D dECM implantation in TBI mice by reducing glial scarring, facilitating neuroblast activation, and stimulating angiogenesis—highlighting its potential as an effective biomaterial for facilitating tissue-level repair following brain injury.

2.6. BDNF loading enhances the ability of 3D dECM to preserve vascularized nerve tissue at the cortical lesion site

After examining the area surrounding the lesion site, we next evaluated the effect of BDNF loading on the efficacy of 3D dECM implantation at the cortical lesion directly affected by physical trauma. To enable tracking, the 3D dECM was fluorescently labeled with cyanine 3 (Cy3) before implantation into TBI mice [28]. At 14 dpi, Cy3 signals remained detectable in both the groups treated with plain 3D dECM and BDNF-loaded 3D dECM (Fig. 7a). The dot-like distribution pattern of the Cy3 signal indicated that the implanted 3D dECM, regardless of BDNF loading, underwent remodeling and disintegration by the host cells, thereby integrating into the local tissue (Fig. 7a).

However, significant differences were observed in the Tuj1-positive fluorescence, indicative of the presence of neurons, between the two groups (Fig. 7a). In the plain 3D dECM-treated group, Tuj1 signals were present in certain areas around the implant, but appeared diffuse, indicating an impaired neurite structure. Conversely, the BDNF-loaded 3D dECM-treated group displayed abundant Tuj1 signals with a clearly defined bundled fiber morphology, indicating a preserved neurite structure.

In addition to examining neuronal structures, we also assessed vascular structures at the implantation site. Immunostaining results (Fig. 7b) revealed that, although CD31-positive lumens were present around the implanted plain 3D dECM, the majority lacked smooth muscle coverage, indicating that these vessels were nascent and immature. Conversely, the BDNF-loaded 3D dECM group showed a higher density of CD31-positive lumens, many of which were covered by smooth muscles, indicating a more mature and stable vascular phenotype. In summary, our findings demonstrated that exogenously loaded BDNF significantly enhances the therapeutic potential of 3D dECM by preserving neuronal morphology and facilitating vascular stability at the cortical lesion site following TBI.

3. Discussion

Cell-derived dECM provides an effective option as a pro-regenerative biomaterial by replicating the characteristics of natural tissue environments and addressing the challenges inherent to tissue-derived dECM [15,39]. In our recent study, we introduced a cell spheroid-derived 3D dECM to overcome the structural limitations of conventional monolayer culture-derived dECM [27,28]. We demonstrated the significant potential of MSC spheroid-derived 3D dECM in mitigating brain injury, attributed to its enriched stem cell matrisome and secretome [28].

Based on these findings, this study further highlights the superior versatility of MSC spheroid-derived 3D dECM for post-decellularization modifications by incorporating growth factors, thereby enabling customized therapeutic potential and functionality for specific applications. As a proof-of-concept, we successfully incorporated the neurotrophic factor BDNF into MSC spheroid-derived 3D dECM, enhancing neuroprotective and proangiogenic properties and resulting in superior brain repair efficacy in a mouse TBI model. Notably, using a mild surfactant during the decellularization process minimized GAG loss compared to that of the strong detergents typically used for preparing tissue-derived dECM. This preservation enabled BDNF loading to rely solely on the intrinsic ability of the native ECM to sequester soluble factors, eliminating the need for chemical or physical modifications. Therefore, this approach provides a straightforward, efficient, and clinically translatable strategy for optimizing the bioactivity of cell spheroid-derived 3D dECM.

Conventionally, tissue-derived dECM is prepared using chemical, physical, or enzymatic approaches, with chemical methods being the most widely employed, specifically those involving detergents [11]. Owing to the tissue thickness, ionic detergents, such as SDS, are especially effective, enabling faster and more thorough decellularization than that of other chemical treatments. For example, SDS has been used for brain tissue decellularization at various concentrations, including 0.3 % [6,32], 0.5 % [30,31], 1 % [33], and 3 % [29], with treatment durations ranging from 24 to 48 h. Although ionic detergents efficiently remove cellular components, they damage ECM bioactive factors and structural proteins, including GAGs, resulting in a significant reduction in the GAG content and associated soluble factors [4,10–15].

In contrast, cell-derived dECM can be prepared using gentler surfactants, such as the nonionic detergent (TX-100) within a significantly shorter time frame (minutes to a few hours). This approach effectively preserves GAGs and associated bioactive molecules, as demonstrated by our *in vitro* results. Additionally, the retained GAG content in cell-derived dECM enhances its capacity to incorporate exogenous growth factors, providing a straightforward and efficient strategy that does not require additional chemical modifications. In this study, we assessed the effects of surfactant treatment on cell spheroid-derived dECM using 0.5 % TX-100 and compared it to 0.3 % SDS for 1 h—a duration significantly shorter than that typically used for brain tissue decellularization. Consequently, the differences in both GAG content and growth factor loading capacity between cell-derived and tissue-derived dECM are likely to be even more significant in practical scenarios. Although tissues can be processed, such as by slicing, to reduce thickness and facilitate decellularization with mild surfactants, conventional challenges of tissue-derived dECM still persist, including xenogeneic source-associated safety concerns and a rigid molecular composition [8,9]. In contrast, cell spheroid-derived 3D dECM offers a safer and more standardized alternative, as it can be engineered from human-sourced cells under controlled processing conditions. Moreover, its composition can be precisely tailored by modulating key parameters such as cell type, spheroid size, oxygen concentration, and culture supplementation, allowing the fine-tuning of bioactivity for diverse regenerative applications [40–43]. This approach provides a robust and flexible strategy for optimizing the properties of cell spheroid-derived 3D dECM, making it a more versatile biomaterial for regenerative applications.

The primary advantage of using MSCs to prepare cell spheroid-derived 3D dECM over other cell types is their inherent stem cell secretome [28], which contains diverse soluble factors that modulate the local niche to create a reparative microenvironment conducive to tissue repair, even without additional post-decellularization modifications. MSC secretome components retained in 3D dECM, identified as having significant potential to counteract the adverse microenvironment, are believed to directly contribute to its therapeutic effects. These

include neurotrophic factors that promote neuroprotection, anti-apoptotic factors, immunomodulatory cytokines, and proangiogenic factors [28], all of which collectively establish a supportive microenvironment for host brain tissues. However, although numerous components of the stem cell secretome are retained during decellularization [28], their levels are inevitably reduced. For example, our previous study reported an approximately 60 % reduction in vascular endothelial growth factor levels [27], and this study revealed an approximately 56 % reduction in BDNF levels in MSC spheroid-derived 3D dECM compared to that in intact MSC spheroids. Additionally, although the MSC secretome facilitates tissue repair, its therapeutic potential may be inherently limited by the insufficient abundance of specific growth factors, even before decellularization.

To address these challenges, post-decellularization incorporation of targeted molecules offers a promising strategy to (i) replenish reduced levels of specific growth factors and (ii) tailor the functionality of MSC spheroid-derived 3D dECM to treat specific diseases or injuries. In this study, BDNF was selected as a representative example to demonstrate the potential of MSC spheroid-derived 3D dECM as an efficient platform for growth factor loading and customization of its therapeutic properties. BDNF, a primary molecule in the development and maintenance of the central nervous system, has been extensively studied for its therapeutic potential in treating TBI [44]. Upon binding to its receptor, tropomyosin receptor kinase B, BDNF activates a cascade of signaling pathways that regulate the expression of genes crucial for neurogenesis and neuronal survival [38]. Beyond these direct neuroprotective effects, emerging evidence has revealed its proangiogenic properties, indicating that BDNF simultaneously supports vascular growth and neuronal repair [45,46]. These diverse roles make BDNF a highly versatile therapeutic candidate for TBI treatment [47–49] and an ideal model growth factor for exploring the incorporation of exogenous factors to optimize the bioactivity and therapeutic potential of MSC spheroid-derived 3D dECM.

As demonstrated in our previous study, 3D dECM retains a wealthy of MSC secretome, including various growth factors and cytokines with significant bioactivities, effectively facilitating brain repair when implanted into TBI mice [28]. In this study, the successful incorporation of exogenous BDNF into the 3D dECM enabled its sustained release, resulting in enhanced neuroprotective, proneuritogenic, and proangiogenic properties directly attributable to the bioactivity of BDNF. These findings highlight the effectiveness of post-decellularization growth factor incorporation in replenishing molecules diminished during decellularization, thereby enhancing the therapeutic potential of the 3D dECM for tissue repair. Additionally, this work serves as a proof-of-concept, highlighting the adaptability of MSC spheroid-derived 3D dECM and demonstrating that its bioactivity can be effectively and readily tuned through a straightforward growth factor loading approach.

Beyond its role in fostering a pro-regenerative microenvironment, 3D dECM may also have potential as a protein-based carrier for growth factor delivery, though this is not the primary focus of the present study. Conventional protein-based carriers, such as collagen, gelatin, and fibrin, typically exhibit limited intrinsic affinity for growth factors and often require ECM-inspired modifications—such as GAG incorporation—to enhance binding efficiency [50–52]. While the addition of growth factor-binding moieties (e.g., heparin [16,53,54] or chondroitin sulfate [55,56]) can improve delivery efficiency, these modifications generally require chemical crosslinking or complex fabrication processes [50–52]. In contrast, the 3D dECM used in this study retains its native GAG content and growth factor-binding domains, enabling the sequestration and gradual release of bioactive molecules without additional modifications. This inherent capability suggests that 3D dECM could serve as a streamlined alternative to conventional protein-based carriers, particularly for tissue repair applications where its intrinsic bioactivity provides additional therapeutic benefits. However, further investigation is warranted to optimize parameters such as 3D dECM size and growth factor loading concentration in order to tailor its application to specific therapeutic scenarios, with the goals of enhancing incorporation efficiency, ensuring sustained release, improving batch-to-batch consistency, and ultimately achieving maximal therapeutic efficacy.

The present study highlights a significant advancement in tailoring the therapeutic potential and versatility of MSC spheroid-derived 3D dECM for tissue repair through post-decellularization incorporation of relevant exogenous molecules. However, key limitations must be addressed for future clinical translation. First, although we have demonstrated the potential of 3D dECM to load and release BDNF, further assessment is required to elucidate the detailed composition of GAGs that survive the decellularization process, remain in the 3D dECM, and contribute to BDNF sequestration. Various GAGs, such as heparin, heparan sulfate, dermatan sulfate, keratan sulfate, and chondroitin sulfate, may be retained in the 3D dECM, each exhibiting distinct charge-mediated interactions and thus binding affinities toward different soluble molecules [50,57]. These interactions are crucial in regulating the loading capacity, release kinetics, and functional activity of incorporated molecules, ultimately influencing not only the therapeutic potential but also the reproducibility of the prepared 3D dECM. Therefore, a comprehensive characterization of GAG composition in 3D dECM will offer valuable insights for optimizing its application in incorporating other growth factors, cytokines, chemokines, or molecules of interest in future studies.

Furthermore, it remains unclear whether the molecules incorporated into the 3D dECM and released upon implantation exert their therapeutic effects in remote tissues by establishing a local concentration gradient or through indirect mechanisms. For example, our *in vivo* observations revealed a higher density of DCX-positive neuroprogenitors in the SVZ of TBI mice treated with BDNF-loaded 3D dECM compared to that in other groups. However, because the 3D dECM was implanted onto the exterior of the damaged cortical tissue, it likely did not directly contact cells in the nearby SVZ region. This indicates the possibility that the observed benefits may result either from a direct BDNF gradient established by the implanted 3D dECM toward the SVZ or from BDNF modulating other cell types, which then indirectly recruits or activates neuroprogenitors. Moreover, investigating how the incorporated molecules are released *in vivo* and how their release correlates with therapeutic effects is crucial for understanding their spatiotemporal dynamics within the injured brain microenvironment. Such insights may help fine-tune the delivery and release strategies of loaded factors, thereby optimizing their release kinetics and enhancing the therapeutic potential of 3D dECM for future regenerative applications.

Additionally, although MSC spheroid-derived 3D dECM has shown promising therapeutic potential in both our previous [28] and present studies, identifying the key components underlying its effects remains essential for clinical translation and optimization. Finally, refining the scalability and batch consistency of 3D dECM production [58], along with growth factor loading, is necessary for broader clinical application. While the spheroid-based approach enables controlled and reproducible fabrication [59], optimizing bioprocessing, decellularization, and growth factor incorporation parameters is crucial for large-scale production. Integrating bioreactor systems and automated manufacturing technologies may improve scalability and consistency while ensuring quality and regulatory compliance [59–61].

4. Conclusion

Based on our previous study, which demonstrated the pro-regenerative potential of both matrisome proteins and secretome inherent in MSC spheroid-derived 3D dECM, this study highlights the feasibility of directly incorporating the desired growth factors, such as BDNF, without requiring additional treatments, such as chemical modifications. This straightforward, efficient, and clinically translatable approach enables the customization and optimization of the bioactivity and therapeutic potential of MSC spheroid-derived 3D dECM, making it a versatile platform for growth factor delivery and regenerative

medicine applications.

5. Materials and methods

5.1. Cell culture

Umbilical cord blood MSCs were purchased from the Bioresource Collection and Research Center, Food Industry Research and Development Institute, Hsinchu, Taiwan, and cultivated in medium as per the supplier's formulation. Specifically, Minimum Essential Medium α (Thermo Fisher Scientific, Waltham, MA, USA) containing 20 % fetal bovine serum (FBS; Corning, Corning, NY, USA) and 4 ng/mL basic fibroblast growth factor (PeproTech, Rocky Hill, NJ, USA) was used. HUVECs, also obtained from the Food Industry Research and Development Institute, were maintained in complete Endothelial Cell Growth Medium-2 (Lonza, Walkersville, MA, USA).

SH-SY5Y neuroblastoma cells were sourced from the American Type Culture Collection (Manassas, VA, USA). For SH-SY5Y cell culture, Dulbecco's Modified Eagle's Medium (DMEM; Thermo Fisher Scientific), prepared with 10 % FBS, 100 U/mL penicillin, 100 μg/mL streptomycin, and 0.25 μg/mL amphotericin B (Corning), was used. Differentiation of SH-SY5Y cells was induced by adding 10 μM retinoic acid (RA; Sigma-Aldrich, St. Louis, MO, USA) [28,62] to the culture medium. The cells were maintained in a humidified incubator at 37 °C with 5 % CO_2.

5.2. Preparation of 3D dECM

To produce 3D dECM, MSC spheroids were generated and decellularized [27,28]. For spheroid formation, a 96-well plate was coated with 50 μL of 12 % (w/v) methylcellulose (Sigma-Aldrich) [27,28,40,41,62–66] dissolved in PBS. Subsequently, trypsinized MSCs (4×10^4) were resuspended in medium containing 25 mg/mL Ficoll 400 (Cytiva, Marlborough, MA, USA) [27,28] and seeded into the wells. After 48 h, MSC spheroids were harvested and incubated for 1 h in a decellularization solution containing either 0.5 % TX-100 with 20 mM ammonium hydroxide [28] or 0.3 % SDS [6,32] on ice, followed by DNase I treatment (1 kU/mL, 37 °C, 4 h; Sigma-Aldrich) to ensure the removal of residual nucleic acids.

To determine the remaining DNA content, the 3D dECM was lysed using RIPA buffer, and the lysates were analyzed using the Quant-iT PicoGreen dsDNA Assay Kit (Thermo Fisher Scientific) according to the manufacturer's instructions. MSC spheroids prior to decellularization served as the control group. For histological evaluation, samples were cryosectioned and stained with H&E. Alternatively, cryosectioned samples were fixed with glutaraldehyde, lyophilized, sputter-coated with platinum, and examined using SEM (JEOL, Tokyo, Japan).

5.3. Quantification of GAG content

To quantify the GAG content in MSC spheroids or the resulting 3D dECM, a Blyscan sulfated GAG assay kit (Biocolor, Belfast, UK) was used following the manufacturer's protocol [27]. Radioimmunoprecipitation assay (RIPA) buffer (20 mM Tris-HCl, 1 mM ethylene glycol-bis(β-aminoethyl ether)-N,N,N′,N′-tetraacetic acid, 150 mM NaCl, and 1 % TX-100), along with a protease inhibitor cocktail (Roche, Basel, Switzerland), was used to lyse MSC spheroids or 3D dECM. After mixing the lysates with Blyscan dye reagent, absorbance was measured at 656 nm using a microplate reader. The GAG concentrations were determined by comparing the absorbance values of the samples with a standard calibration curve.

5.4. 3D dECM for BDNF loading and release

Sixteen 3D dECM pieces were incubated in 200 μL BDNF solution (100 ng/mL; 248-BDB-010, R&D Systems, Minneapolis, MN, USA) dissolved in PBS at room temperature with gentle shaking. Unbound BDNF was removed through three washes with PBS. To assess BDNF levels in test samples, MSC spheroids or 3D dECM were lysed using RIPA buffer with a protease inhibitor cocktail, and the BDNF content was analyzed using ELISA (DBNT00, R&D Systems) or western blotting. For Western blot analysis, the protein lysates were separated on a 15 % SDS-polyacrylamide gel (Bio-Rad Laboratories, Hercules, CA, USA) at 80 V. Proteins were transferred onto a polyvinylidene difluoride membrane, incubated with 5 % skim milk for 1 h, and treated overnight with anti-BDNF primary antibody (GTX132621, GeneTex, Hsinchu, Taiwan). Protein signals were detected using horseradish peroxidase-conjugated secondary antibodies (GeneTex) and Amersham ECL detection reagent (Cytiva). To assess BDNF release, 16 pieces of BDNF-loaded 3D dECM were placed in 200 μL PBS and incubated at 37 °C under gentle agitation. At specific time points, the PBS supernatant was collected for ELISA, and an equal volume of fresh PBS was replenished to maintain the incubation conditions.

5.5. Assessment of the proneuritogenic effects of BDNF-loaded 3D dECM

SH-SY5Y cells were cultured on coverslips in RA-supplemented medium for 5 days to induce differentiation. Subsequently, the cells were treated for 3 days in RA-free medium with either plain 3D dECM, free BDNF (100 ng/mL), or BDNF-loaded 3D dECM. Neurite morphology was assessed by immunofluorescence staining with a Tuj1 antibody (10094-1-AP, Proteintech, Rosemont, IL, USA). Images were captured with a fluorescence microscope (20 × objective lens), selecting five random fields per sample. Neurite lengths were measured for ten cells per field, and both the neurite lengths were determined using the ImageJ software with the NeuronJ plugin [67–69].

Alternatively, trypsinized SH-SY5Y cells (8×10^5) were suspended in medium along with 40 pieces of plain 3D dECM or BDNF-loaded 3D dECM in tubes and incubated at 37 °C to facilitate cell attachment. After 4 h, the 3D dECM was rinsed thrice with prewarmed PBS to remove unattached cells, transferred to an ultra-low attachment plate (Corning), and cultured in RA-supplemented medium for 4 days. Neurite morphology was analyzed by immunofluorescence staining with a Tuj1 antibody, and the samples were visualized using a confocal microscope.

5.6. Assessment of the neuroprotective effects of BDNF-loaded 3D dECM

SH-SY5Y cells were cultured in RA-supplemented medium for 5 days to facilitate differentiation. The medium was then replaced with fresh medium containing 80 mM glutamate and supplemented with plain 3D dECM, free BDNF (100 ng/mL), or BDNF-loaded 3D dECM. After 24 h of incubation, cell viability was evaluated using the CCK-8 assay (Abbkine, Atlanta, GA, USA), and neurite morphology was assessed using Tuj1 immunostaining.

5.7. Assessment of the proangiogenic effects of BDNF-loaded 3D dECM

HUVECs were plated onto a growth factor-reduced Matrigel-coated surface (BD Biosciences, San Jose, CA, USA) in DMEM containing 10 % FBS [70]. After 4 h of incubation, plain 3D dECM, free BDNF (100 ng/mL), or BDNF-loaded 3D dECM was introduced into the culture system. The development of tubular networks by HUVECs was monitored, and the microscopic images were analyzed using the ImageJ software to quantify the tube lengths.

5.8. Implantation of BDNF-loaded 3D dECM into a mouse model of TBI

All animal experiments adhered to the ARRIVE 2.0 guidelines and Guidelines for the Care and Use of Laboratory Animals (2018) set by the Council of Agriculture, Executive Yuan, Taiwan. The experimental protocol was approved by the Institutional Animal Care and Use Committee (IACUC) of National Tsing Hua University, Hsinchu, Taiwan

(Approval No. 110013). Male C57BL/6J mice (8 weeks old, BioLASCO, Taipei, Taiwan) were housed at the university's Laboratory Animal Center under a 12-h light/dark cycle with unrestricted access to food and water.

To establish a mouse TBI model, animals were anesthetized through intraperitoneal administration of avertin (200 mg/kg body weight)—prepared as a 1.25 % solution of 2,2,2-tribromoethanol in PBS containing 2.5 % 2-methyl-2-butanol (Sigma-Aldrich) [28]. Subsequently, a 3 mm circular section of the skull was carefully removed through craniectomy, targeting the left cortical hemisphere at coordinates 1.0 mm posterior and 2.0 mm lateral to the bregma. A cortical impactor (Custom Design & Fabrication, Sandston, VA, USA) employing a tip measuring 2 mm in diameter, delivering an impact at a velocity of 5 m/s, depth of 2 mm, and dwell time of 250 ms [28] to induce severe TBI [28,71,72]. Animals that underwent craniectomy without cortical impact served as healthy controls. Following cortical impact and hemostasis, the animals were divided into treatment groups using a list randomizer. To immobilize the treatment materials, 20 μL of fibrin gel formulated with 6.25 mg/mL fibrinogen and 25 U/mL thrombin (Sigma-Aldrich) was applied [28]. The treatment groups consisted of: (1) 20 pieces of plain 3D dECM, (2) free BDNF at a final concentration of 100 ng/mL, or (3) 20 pieces of BDNF-loaded 3D dECM, with six animals per group. The 3D dECM was pre-labeled with Cy3 by incubating it with Cy3 *N*-hydroxysuccinimide ester (Abcam, Cambridge, MA, USA) [28] for tracing. The control group received plain fibrin gel alone, without any additional materials. Once the fibrin gel solidified, the wound was closed with sutures to ensure proper sealing.

The neurological functions of the test mice were evaluated 1 day prior to model creation and at 1, 4, and 7 days dpi by assessing their mNSS, foot faults during grid walking, and ability to maintain balance on a rotating rod, following the protocol described in our recent publication [28].

5.9. Histological analysis

On day 14 post-injury, the animals were euthanized through transcardiac perfusion with cold PBS, followed by 4 % paraformaldehyde. The brains were dissected, fixed overnight in 4 % paraformaldehyde, cryoprotected by immersion in 10 % sucrose for 1 h, and then in 30 % sucrose until the tissues settled. FSC 22 Frozen Section Media (Leica Biosystems, Wetzlar, Germany) was used to embed the tissues, which were then frozen in pre-cooled 2-methylbutane on dry ice. A cryostat microtome (Leica Biosystems) was used to prepare thin coronal brain sections (10 μm).

Lesion size was assessed by cresyl violet staining of the sections at 60 °C for 10 min. After mounting and scanning, the lesion volume (%) was measured using the ImageJ software based on the following formula: ([contralateral hemisphere volume − ipsilateral hemisphere volume]/contralateral hemisphere volume) × 100. Additionally, sections were immunostained with primary antibodies specific to CD31 (BD Biosciences, 550274), DCX (Proteintech, 13925-1-AP), GFAP (Proteintech, 16825-1-AP), or Tuj1 (Proteintech, 10094-1-AP) and visualized using the corresponding secondary antibodies. The stained sections were analyzed by fluorescence or confocal microscopy. To identify glial scars, neuroblasts, or blood vessels, five fields, randomly selected around the injury region, were captured at 20 × magnification on each slide.

5.10. Statistical analysis

GraphPad Prism software (version 10.4.1; San Diego, CA, USA) was used for data analysis, and the results are expressed as the mean ± standard deviation. One-way analysis of variance with Tukey's *post hoc* test was applied for comparisons involving three or more groups. Statistical significance was set at $p < 0.05$.

CRediT authorship contribution statement

Ying-Chi Kao: Writing – original draft, Visualization, Validation, Methodology, Investigation, Formal analysis, Conceptualization. **Pei-Ching Yang:** Visualization, Validation, Methodology, Investigation, Formal analysis. **Yu-Ping Lin:** Visualization, Validation, Methodology, Investigation. **Grace H. Chen:** Methodology, Investigation, Formal analysis. **Shao-Wen Liu:** Methodology, Investigation. **Chia-Hsin Ho:** Methodology, Investigation. **Shih-Chen Huang:** Investigation. **Peng-Ying Lee:** Investigation. **Linyi Chen:** Resources, Methodology. **Chieh-Cheng Huang:** Writing – review & editing, Supervision, Resources, Project administration, Funding acquisition, Conceptualization.

Declaration of competing interest

The authors declare the following financial interests/personal relationships which may be considered as potential competing interests: Chieh-Cheng Huang reports financial support was provided by National Health Research Institutes. Chieh-Cheng Huang reports financial support was provided by National Science and Technology Council. If there are other authors, they declare that they have no known competing financial interests or personal relationships that could have appeared to influence the work reported in this paper.

Acknowledgements

This work was supported by the National Health Research Institutes (NHRI-EX113-11131EI), the National Science and Technology Council of Taiwan (NSTC 111-2628-B-007-004 and NSTC 113-2221-E-007-019-MY3) and National Tsing Hua University (114QF028E1).

Appendix A. Supplementary data

Supplementary data to this article can be found online at https://doi.org/10.1016/j.biomaterials.2025.123332.

Data availability

Data will be made available on request.

References

[1] K. Blennow, D. Brody, P. Kochanek, et al., Traumatic brain injuries, Nat. Rev. Dis. Primers 2 (2016) 16084, https://doi.org/10.1038/nrdp.2016.84.
[2] D.W. Simon, M.J. McGeachy, H. Bayir, et al., The far-reaching scope of neuroinflammation after traumatic brain injury, Nat. Rev. Neurol. 13 (3) (2017) 171–191, https://doi.org/10.1038/nrneurol.2017.13.
[3] G. Orive, E. Anitua, J.L. Pedraz, et al., Biomaterials for promoting brain protection, repair and regeneration, Nat. Rev. Neurosci. 10 (9) (2009) 682–692, https://doi.org/10.1038/nrn2685.
[4] M. Brown, J. Li, C. Moraes, et al., Decellularized extracellular matrix: new promising and challenging biomaterials for regenerative medicine, Biomaterials 289 (2022) 121786, https://doi.org/10.1016/j.biomaterials.2022.121786.
[5] Y. Wu, J. Wang, Y. Shi, et al., Implantation of brain-derived extracellular matrix enhances neurological recovery after traumatic brain injury, Cell Transplant. 26 (7) (2017) 1224–1234, https://doi.org/10.1177/0963689717714090.
[6] B. Kim, J. Kim, J. Lee, et al., Decellularized brain extracellular matrix based NGF-Releasing cryogel for brain tissue engineering in traumatic brain injury, J. Contr. Release 368 (2024) 140–156, https://doi.org/10.1016/j.jconrel.2024.02.017.
[7] S. Li, J. Xu, Y. Qian, et al., Hydrogel in the treatment of traumatic brain injury, Biomater. Res. 28 (2024) 85, https://doi.org/10.34133/bmr.0085.
[8] M. Kasravi, A. Ahmadi, A. Babajani, et al., Immunogenicity of decellularized extracellular matrix scaffolds: a bottleneck in tissue engineering and regenerative medicine, Biomater. Res. 27 (1) (2023) 10, https://doi.org/10.1186/s40824-023-00348-z.
[9] M. Massaro, R. Pálek, J. Rosendorf, et al., Decellularized xenogeneic scaffolds in transplantation and tissue engineering: immunogenicity versus positive cell stimulation, Mater. Sci. Eng., C 127 (2021) 112203, https://doi.org/10.1016/j.msec.2021.112203.
[10] D. Faulk, C. Carruthers, H. Warner, et al., The effect of detergents on the basement membrane complex of a biologic scaffold material, Acta Biomater. 10 (2014) 183–193, https://doi.org/10.1016/j.actbio.2013.09.006.

[11] D. Moffat, K. Ye, S. Jin, Decellularization for the retention of tissue niches, J. Tissue Eng. 13 (2022) 1–29, https://doi.org/10.1177/20417314221101151.
[12] J. Fernández-Pérez, M. Ahearne, The impact of decellularization methods on extracellular matrix derived hydrogels, Sci. Rep. 9 (2019) 14933, https://doi.org/10.1038/s41598-019-49575-2.
[13] T. Liguori, G. Liguori, J. van Dongen, et al., Bioactive decellularized cardiac extracellular matrix-based hydrogel as a sustained-release platform for human adipose tissue-derived stromal cell-secreted factors, Biomed. Mater. 16 (2021) 025022, https://doi.org/10.1088/1748-605X/abcff9.
[14] J. Willemse, M. Verstegen, A. Vermeulen, et al., Fast, robust and effective decellularization of whole human livers using mild detergents and pressure controlled perfusion, Mater. Sci. Eng., C 108 (2020) 110200, https://doi.org/10.1016/j.msec.2019.110200.
[15] H. Chen, S. Zhang, Y. Fu, Emerging strategies for optimizing cell-derived decellularized extracellular matrix scaffolds in tissue engineering, Adv. Eng. Mater. 26 (2024) 2302148, https://doi.org/10.1002/adem.202302148.
[16] A. Rindone, B. Kachniarz, C. Achebe, et al., Heparin-conjugated decellularized bone particles promote enhanced osteogenic signaling of PDGF-bb to adipose-derived stem cells in tissue engineered bone grafts, Adv. Healthcare Mater. 8 (10) (2019) 1801565, https://doi.org/10.1002/adhm.201801565.
[17] I. Kim, M. Hwang, P. Du, et al., Bioactive cell-derived matrices combined with polymer mesh scaffold for osteogenesis and bone healing, Biomaterials 50 (2015) 75–86, https://doi.org/10.1016/j.biomaterials.2015.01.054.
[18] M. Parmaksiz, Decellularized tendon-based heparinized nanocomposite scaffolds for prospective regenerative applications: Chemical, physical, thermal, mechanical and *in vitro* biological evaluations, J. Mech. Behav. Biomed. Mater. 134 (2022) 105387, https://doi.org/10.1016/j.jmbbm.2022.105387.
[19] Q. Lu, M. Li, Y. Zou, et al., Delivery of basic fibroblast growth factors from heparinized decellularized adipose tissue stimulates potent de novo adipogenesis, J. Contr. Release 174 (2014) 43–50, https://doi.org/10.1016/j.jconrel.2013.11.007.
[20] L. Zhou, Z. Wang, Z. Wang, et al., Effect of heparinization on promoting angiogenesis of decellularized kidney scaffolds, J. Biomed. Mater. Res. 109 (10) (2021) 1979–1989, https://doi.org/10.1002/jbm.a.37190.
[21] X. Kong, C. Kong, S. Wen, et al., The use of heparin, bFGF, and VEGF 145 grafted acellular vascular scaffold in small diameter vascular graft, J. Biomed. Mater. Res. B Appl. Biomater. 107 (3) (2019) 672–679, https://doi.org/10.1002/jbm.b.34160.
[22] S. Zhang, Q. Lu, T. Cao, et al., Adipose tissue and extracellular matrix development by injectable decellularized adipose matrix loaded with basic fibroblast growth factor, Plast. Reconstr. Surg. 137 (4) (2016) 1171–1180, https://doi.org/10.1097/PRS.0000000000002019.
[23] K. Liu, M. Zhao, Y. Li, et al., VEGF loaded porcine decellularized adipose tissue derived hydrogel could enhance angiogenesis *In vitro* and *In vivo*, J. Biomater. Sci. Polym. Ed. 33 (5) (2022) 569–589, https://doi.org/10.1080/09205063.2021.2002235.
[24] Y. Ostadi, J. Khanali, F. Tehrani, et al., Decellularized extracellular matrix scaffolds for soft tissue augmentation: from host-scaffold interactions to bottlenecks in clinical translation, Biomater. Res. 28 (2024) 71, https://doi.org/10.34133/bmr.0071.
[25] Q. Wu, Y. Li, Y. Wang, et al., The effect of heparinized decellularized scaffolds on angiogenic capability, J. Biomed. Mater. Res. 104 (12) (2016) 3021–3030, https://doi.org/10.1002/jbm.a.35843.
[26] M. Song, Y. Zhou, Y. Liu, VEGF heparinized-decellularized adipose tissue scaffolds enhance tissue engineering vascularization *in vitro*, RSC Adv. 8 (59) (2018) 33614–33624, https://doi.org/10.1039/c7ra13282d.
[27] C.E. Chiang, Y.Q. Fang, C.T. Ho, et al., Bioactive decellularized extracellular matrix derived from 3D stem cell spheroids under macromolecular crowding serves as a scaffold for tissue engineering, Adv. Healthcare Mater. 10 (2021) 2100024, https://doi.org/10.1002/adhm.202100024.
[28] G. Chen, K. Sia, S. Liu, et al., Implantation of MSC spheroid-derived 3D decellularized ECM enriched with the MSC secretome ameliorates traumatic brain injury and promotes brain repair, Biomaterials 315 (2025) 122941, https://doi.org/10.1016/j.biomaterials.2024.122941.
[29] Y. Jin, J. Lee, J. Kim, et al., Three-dimensional brain-like microenvironments facilitate the direct reprogramming of fibroblasts into therapeutic neurons, Nat. Biomed. Eng. 2 (7) (2018) 522–539, https://doi.org/10.1038/s41551-018-0260-8.
[30] M. Bae, H. Ngo, Y. Kang, et al., Laminin-augmented decellularized extracellular matrix ameliorating neural differentiation and neuroinflammation in human mini-brains, Small 20 (23) (2024) 2308815, https://doi.org/10.1002/smll.202308815.
[31] M. Bae, D. Hwang, M. Ko, et al., Neural stem cell delivery using brain-derived tissue-specific bioink for recovering from traumatic brain injury, Biofabrication 13 (2021) 044110, https://doi.org/10.1088/1758-5090/ac293f.
[32] H. Han, S. Lee, G. Gao, et al., Cerebrovascular-specific extracellular matrix bioink promotes blood-brain barrier properties, Biomater. Res. 28 (2024) 115, https://doi.org/10.34133/bmr.0115.
[33] A. Granato, E. da Cruz, D. Rodrigues, et al., A novel decellularization method to produce brain scaffolds, Tissue Cell 67 (2020) 101412, https://doi.org/10.1016/j.tice.2020.101412.
[34] M. Zurita, L. Otero, C. Aguayo, et al., Cell therapy for spinal cord repair: optimization of biologic scaffolds for survival and neural differentiation of human bone marrow stromal cells, Cytotherapy 12 (2010) 522–537, https://doi.org/10.3109/14653241003615164.
[35] S. Pan, Z. Qi, Q. Li, et al., Graphene oxide-PLGA hybrid nanofibres for the local delivery of IGF-1 and BDNF in spinal cord repair, Artif. Cells, Nanomed. Biotechnol. 47 (2019) 651–664, https://doi.org/10.1080/21691401.2019.1575843.
[36] T. Mishchenko, M. Klimenko, A. Kuznetsova, et al., 3D-printed hyaluronic acid hydrogel scaffolds impregnated with neurotrophic factors (BDNF, GDNF) for post-traumatic brain tissue reconstruction, Front. Bioeng. Biotechnol. 10 (2022) 895406, https://doi.org/10.3389/fbioe.2022.895406.
[37] A. Sandoval-Castellanos, F. Claeyssens, J. Haycock, Biomimetic surface delivery of NGF and BDNF to enhance neurite outgrowth, Biotechnol. Bioeng. 117 (10) (2020) 3124–3135, https://doi.org/10.1002/bit.27466.
[38] N. Wu, X. Sun, C. Zhou, et al., Neuroblasts migration under control of reactive astrocyte-derived BDNF: a promising therapy in late neurogenesis after traumatic brain injury, Stem Cell Res. Ther. 14 (2023) 2, https://doi.org/10.1186/s13287-022-03232-0.
[39] G.S. Hussey, J.L. Dziki, S.F. Badylak, Extracellular matrix-based materials for regenerative medicine, Nat. Rev. Mater. 3 (7) (2018) 159–173, https://doi.org/10.1038/s41578-018-0023-x.
[40] W.Y. Yang, L.C. Chen, Y.T. Jhuang, et al., Injection of hybrid 3D spheroids composed of podocytes, mesenchymal stem cells, and vascular endothelial cells into the renal cortex improves kidney function and replenishes glomerular podocytes, Bioeng. Transl. Med. 6 (2) (2021) e10212, https://doi.org/10.1002/btm2.10212.
[41] L.C. Chen, H.W. Wang, C.C. Huang, Modulation of inherent niches in 3D multicellular MSC spheroids reconfigures metabolism and enhances therapeutic potential, Cells 10 (10) (2021) 2747, https://doi.org/10.3390/cells10102747.
[42] K.H. Griffin, S.W. Fok, J.K. Leach, Strategies to capitalize on cell spheroid therapeutic potential for tissue repair and disease modeling, NPJ Regen. Med. 7 (1) (2022) 70, https://doi.org/10.1038/s41536-022-00266-z.
[43] N. Herger, I. Heggli, T. Mengis, et al., Impacts of priming on distinct immunosuppressive mechanisms of mesenchymal stromal cells under translationally relevant conditions, Stem Cell Res. Ther. 15 (1) (2024) 65, https://doi.org/10.1186/s13287-024-03677-5.
[44] L. Giesler, R. Mychasiuk, S. Shultz, et al., BDNF: new views of an old player in traumatic brain injury, Neuroscientist 30 (2024) 560–573, https://doi.org/10.1177/10738584231164918.
[45] T. Usui, A. Naruo, M. Okada, et al., Brain-derived neurotrophic factor promotes angiogenic tube formation through generation of oxidative stress in human vascular endothelial cells, Acta Physiol. 211 (2014) 385–394, https://doi.org/10.1111/apha.12249.
[46] P. Kermani, D. Rafii, D. Jin, et al., Neurotrophins promote revascularization by local recruitment of TrkB+ endothelial cells and systemic mobilization of hematopoietic progenitors, J. Clin. Investig. 115 (2005) 653–663, https://doi.org/10.1172/JCI200522655.
[47] W. Guo, K. Liu, Y. Wang, et al., Neurotrophins and neural stem cells in posttraumatic brain injury repair, animal model exp, Med. 7 (1) (2024) 12–23, https://doi.org/10.1002/ame2.12363.
[48] D. Gustafsson, A. Klang, S. Thams, et al., The role of BDNF in experimental and clinical traumatic brain injury, Int. J. Mol. Sci. 22 (7) (2021) 3582, https://doi.org/10.3390/ijms22073582.
[49] E. Atkinson, R. Dickman, Growth factors and their peptide mimetics for treatment of traumatic brain injury, Bioorg. Med. Chem. 90 (2023) 117368, https://doi.org/10.1016/j.bmc.2023.117368.
[50] D. Hachim, T.E. Whittaker, H. Kim, et al., Glycosaminoglycan-based biomaterials for growth factor and cytokine delivery: making the right choices, J. Contr. Release 313 (2019) 131–147, https://doi.org/10.1016/j.jconrel.2019.10.018.
[51] M. Martino, P. Briquez, K. Maruyama, et al., Extracellular matrix-inspired growth factor delivery systems for bone regeneration, Adv. Drug Deliv. Rev. 94 (2015) 41–52, https://doi.org/10.1016/j.addr.2015.04.007.
[52] R. Gresham, C. Bahney, J. Leach, Growth factor delivery using extracellular matrix-mimicking substrates for musculoskeletal tissue engineering and repair, Bioact. Mater. 6 (7) (2021) 1945–1956, https://doi.org/10.1016/j.bioactmat.2020.12.012.
[53] M. Hettiaratchi, L. Krishnan, T. Rouse, et al., Heparin-mediated delivery of bone morphogenetic protein-2 improves spatial localization of bone regeneration, Sci. Adv. 6 (1) (2020) eaay1240, https://doi.org/10.1126/sciadv.aay1240.
[54] M. Lee, T. Ahmad, J. Lee, et al., Dual delivery of growth factors with coacervate-coated poly(lactic-*co*-glycolic acid) nanofiber improves neovascularization in a mouse skin flap model, Biomaterials 124 (2017) 65–77, https://doi.org/10.1016/j.biomaterials.2017.01.036.
[55] C. Latchoumane, M. Betancur, G. Simchick, et al., Engineered glycomaterial implants orchestrate large-scale functional repair of brain tissue chronically after severe traumatic brain injury, Sci. Adv. 7 (10) (2021) eabe0207, https://doi.org/10.1126/sciadv.abe0207.
[56] S. Andrews, A. Cheng, H. Stevens, et al., Chondroitin sulfate glycosaminoglycan scaffolds for cell and recombinant protein-based bone regeneration, Stem Cells Transl. Med. 8 (6) (2019) 575–585, https://doi.org/10.1002/sctm.18-0141.
[57] F. Zhang, L. Zheng, S. Cheng, et al., Comparison of the interactions of different growth factors and glycosaminoglycans, Molecules 24 (2019) 3360, https://doi.org/10.3390/molecules24183360.
[58] D.H. Ramos-Rodriguez, J.K. Leach, Decellularized cell-secreted extracellular matrices as biomaterials for tissue engineering, Small Sci 5 (2) (2025) 2400335, https://doi.org/10.1002/smsc.202400335.
[59] T. Zhu, Y. Hu, H. Cui, et al., 3D multispheroid assembly strategies towards tissue engineering and disease modeling, Adv. Healthcare Mater. 13 (23) (2024) 2400957, https://doi.org/10.1002/adhm.202400957.
[60] A. Mehesz, J. Brown, Z. Hajdu, et al., Scalable robotic biofabrication of tissue spheroids, Biofabrication 3 (2) (2011) 025002, https://doi.org/10.1088/1758-5082/3/2/025002.

[61] I. Grexa, A. Diosdi, A. Kriston, et al., SpheroidPicker for automated 3D cell culture manipulation using deep learning, Sci. Rep. 11 (1) (2021) 14813, https://doi.org/10.1038/s41598-021-94217-1.
[62] Y.J. Lin, Y.W. Lee, C.W. Chang, et al., 3D spheroids of umbilical cord blood MSC-derived Schwann cells promote peripheral nerve regeneration, Front. Cell Dev. Biol. 8 (1632) (2020) 604946, https://doi.org/10.3389/fcell.2020.604946.
[63] C.P. Yu, J.H. Juang, Y.J. Lin, et al., Enhancement of subcutaneously transplanted β cell survival using 3D stem cell spheroids with proangiogenic and prosurvival potential, Adv. Biosys. 4 (3) (2020) 1900254, https://doi.org/10.1002/adbi.201900254.
[64] S.H. Chen, Y.W. Lee, H.K. Kao, et al., The transplantation of 3-dimensional spheroids of adipose-derived stem cells promotes achilles tendon healing in rabbits by enhancing the proliferation of tenocytes and suppressing M1 macrophages, Am. J. Sports Med. 52 (2) (2024) 406–422, https://doi.org/10.1177/03635465231214698.
[65] S.H. Chen, H.W. Wang, P.C. Yang, et al., Schwann cells acquire a repair phenotype after assembling into spheroids and show enhanced *In vivo* therapeutic potential for promoting peripheral nerve repair, Bioeng. Transl. Med. 9 (2024) e10635, https://doi.org/10.1002/btm2.10635.
[66] T.W. Hsu, Y.J. Lu, Y.J. Lin, et al., Transplantation of 3D MSC/HUVEC spheroids with neuroprotective and proangiogenic potentials ameliorates ischemic stroke brain injury, Biomaterials 272 (2021) 120765, https://doi.org/10.1016/j.biomaterials.2021.120765.
[67] I. Poudel, J. Lee, L. Tan, et al., Micropatterning-retinoic acid co-control of neuronal cell morphology and neurite outgrowth, Acta Biomater. 9 (1) (2013) 4592–4598, https://doi.org/10.1016/j.actbio.2012.08.039.
[68] Z. Lu, C. Barberio, A. Fernandez-Villegas, et al., Microelectrode arrays measure blocking of voltage-gated calcium ion channels on supported lipid bilayers derived from primary neurons, Adv. Sci. 11 (27) (2024) 2304301, https://doi.org/10.1002/advs.202304301.
[69] C. Barberio, J. Saez, A. Withers, et al., Conducting polymer-ECM scaffolds for human neuronal cell differentiation, Adv. Healthcare Mater. 11 (20) (2022) 2200941, https://doi.org/10.1002/adhm.202200941.
[70] C.C. Huang, C.K. Chang, P.C. Yang, et al., Injectable glucose-releasing microgels enhance the survival and therapeutic potential of transplanted MSCs under ischemic conditions, Adv. Healthcare Mater. 14 (6) (2025) 2401724, https://doi.org/10.1002/adhm.202401724.
[71] X. Ma, A. Aravind, B. Pfister, et al., Animal models of traumatic brain injury and assessment of injury severity, Mol. Neurobiol. 56 (8) (2019) 5332–5345, https://doi.org/10.1007/s12035-018-1454-5.
[72] M. Liang, T. Lu, L. Chen, Timely expression of PGAM5 and its cleavage control mitochondrial homeostasis during neurite re-growth after traumatic brain injury, Cell Biosci. 13 (1) (2023) 96, https://doi.org/10.1186/s13578-023-01052-0.